



HAL
open science

Zinc alleviates pain through high-affinity binding to the NMDA receptor NR2A subunit

Chihiro Nozaki, Angela Maria Maria Vergnano, Dominique Filliol, Abdel-Moultalib Ouagazzal, Anna Le Goff, Stéphanie Carvalho, David Reiss, Claire Gavériaux-Ruff, Jacques Neyton, Pierre Paoletti, et al.

► To cite this version:

Chihiro Nozaki, Angela Maria Maria Vergnano, Dominique Filliol, Abdel-Moultalib Ouagazzal, Anna Le Goff, et al.. Zinc alleviates pain through high-affinity binding to the NMDA receptor NR2A subunit. Nature Neuroscience, 2011, 10.1038/nn.2844 . hal-00655884

HAL Id: hal-00655884

<https://hal.science/hal-00655884>

Submitted on 3 Jan 2012

HAL is a multi-disciplinary open access archive for the deposit and dissemination of scientific research documents, whether they are published or not. The documents may come from teaching and research institutions in France or abroad, or from public or private research centers.

L'archive ouverte pluridisciplinaire **HAL**, est destinée au dépôt et à la diffusion de documents scientifiques de niveau recherche, publiés ou non, émanant des établissements d'enseignement et de recherche français ou étrangers, des laboratoires publics ou privés.

Zinc alleviates pain through high-affinity binding to the NMDA receptor NR2A subunit

Chihiro Nozaki^{1*}, Angela Maria Vergnano^{2*}, Dominique Filliol¹, Abdel-Mouttalib Ouagazzal¹, Anne Le Goff², Stéphanie Carvalho², David Reiss¹, Claire Gaveriaux-Ruff¹, Jacques Neyton², Pierre Paoletti^{2§} and Brigitte L. Kieffer^{1§}

¹Institut de Génétique et de Biologie Moléculaire et Cellulaire, Centre National de la Recherche Scientifique/Institut National de la Santé et de la Recherche Médicale/Université de Strasbourg, 1 Rue Laurent Fries, 67404 Illkirch, France. ²Ecole Normale Supérieure, Institut de Biologie de l'Ecole Normale Supérieure (IBENS), CNRS UMR8197, INSERM U1024, 46 rue d'Ulm, 75005 Paris, France.

*equal contributors

§These authors jointly directed the work

§To whom correspondence should be sent:

Dr. Pierre Paoletti

Institut de Biologie de l'Ecole Normale Supérieure

Section Neuroscience

46 rue d'Ulm, 75005 Paris, France.

Tel 33 (0)1 44 32 38 94

Fax 33(0)1 44 32 38 87

e-mail pierre.paoletti@ens.fr

Abstract

Zinc is abundant in the central nervous system and regulates pain, but underlying mechanisms are unknown. *In vitro* studies have shown that extracellular zinc modulates a plethora of signaling membrane proteins including NMDA receptors containing the NR2A subunit, which display exquisite zinc sensitivity. We created NR2A-H128S knock-in mice to investigate whether Zn²⁺-NR2A interaction influences pain control. In these mice, high-affinity (nanomolar) zinc inhibition of NMDA currents was lost in hippocampus and spinal cord. Knock-in mice showed hypersensitivity to radiant heat and capsaicin, and developed enhanced allodynia in inflammatory and neuropathic pain models. Furthermore, zinc-induced analgesia was completely abolished under both acute and chronic pain conditions. Our data establish that zinc is an endogenous modulator of excitatory neurotransmission *in vivo*, and identify a novel mechanism in pain processing that relies on NR2A NMDA receptors. The study also provides a molecular basis for pain-relieving effects of dietary zinc supplementation.

Zinc is essential for life and is the second most prevalent trace element in the body after iron. This heavy metal is critically involved in cellular metabolism, and detrimental consequences of zinc deficiency in human nutrition and public health are well recognized since 1960s¹. Most zinc is bound to metalloproteins, and contributes to enzymatic catalysis or structural stability¹. Zinc is particularly abundant in the central nervous system. Intriguingly, a significant amount of neural zinc (~10%) is found in axon terminals of neurons in a chelatable ionic form (Zn^{2+})². CNS chelatable Zn^{2+} is mostly sequestered in synaptic vesicles of glutamatergic neurons, and Zn^{2+} co-release with glutamate has been proposed to modulate both excitatory and inhibitory synaptic transmission and plasticity³⁻⁶. This observation led many authors to propose a role for zinc in brain function, such as motor control⁷ and neurological disorders^{2,8}, including pathological pain^{9,10}. At present, however, the physiological significance of synaptic zinc remains largely unknown. A major hurdle in the study of synaptic zinc physiology is the myriad of potential zinc targets, which include several voltage-dependent ion channels, and major neurotransmitter transporters and receptors^{8,11-13}. On these targets, zinc can exert either positive or negative modulatory effects with degrees of potency that vary considerably. Effects of zinc are thus expected to be multiple and complex, both increasing and decreasing neuronal excitability.

In vitro, NMDA receptors (NMDARs) have been identified as one of the potential synaptic targets for zinc effects on excitatory transmission^{11,13}. NMDARs play key roles in both physiology and pathology of the nervous system¹⁴. Notably these receptors highly contribute to pain transmission and play a major role in the development of chronic pain^{15,16}. NMDARs are heteromeric assemblies composed mainly of NR1 and NR2 subunits, and form glutamate-gated ion channels with biophysical and pharmacological properties largely determined by the type of NR2 subunit (A to D)¹⁴. In particular the NR2A subunit, which is widely expressed in the adult nervous system, confers to NMDARs exquisite sensitivity for extracellular zinc. The NR2A clamshell-like N-terminal domain contains a high-affinity Zn^{2+} binding site, which mediates allosteric inhibition of NR2A-containing NMDARs by nanomolar zinc concentrations^{17,18}. Functional and modeling studies on recombinant NMDARs have identified several residues that are essential for Zn^{2+} binding to the NR2A N-terminal domain. This is the case for histidine 128, whose mutation strongly reduces Zn^{2+} affinity (~1000-fold shift in IC_{50}) while other receptor properties, including agonist (glutamate and glycine) sensitivity, channel maximal open probability, Mg^{2+} block and proton inhibition are unaffected¹⁸⁻²¹. To investigate the importance of zinc action on NMDARs *in vivo*, we generated mutant mice carrying the H128S mutation on the NMDAR NR2A subunit.

Here we demonstrate that the Zn^{2+} -NR2A interaction is a key molecular event regulating major aspects of pain processing.

RESULTS AND DISCUSSION

Generation and characterization of NR2A H128S knock-in mice

We generated knock-in mutant mice harboring a histidine-to-serine point mutation at position 128 of the NR2A subunit (NR2A-H128S mutation) to assess the physiological relevance of Zn^{2+} acting at NR2A subunits *in vivo*. We used homologous recombination to introduce the desired mutation into the NR2A gene of mouse embryonic stem cells²², and obtained the NR2A-H128S knock-in mouse line (**Fig. 1**).

We first assessed effects of the NR2A-H128S mutation at the tissue level (**Fig. 2**). To determine whether NMDARs from NR2A-H128S mutant mice are insensitive to low (nM) zinc concentrations, we transplanted forebrain membrane extracts into *Xenopus* oocytes and measured resulting NMDA currents. High-affinity zinc inhibition of NMDA currents was lost (**Fig. 2a**), demonstrating that the targeting strategy was successful. Furthermore, sensitivity to ifenprodil, a NR2B-selective antagonist¹⁴, was indistinguishable between wild-type and knock-in preparations, indicating that proportions of NR2A vs NR2B subunits were maintained in mutant mice (**Fig. 2a**). We then measured excitatory post-synaptic NMDA currents (NMDA EPSCs) in acute slices from hippocampus, which possess zinc-containing neuron terminals at high density^{2, 8}, and spinal cord as a main site for pain processing. In both slice preparations, and in line with our observation in oocytes, NMDA EPSCs from wild-type animals were markedly inhibited by exogenous submicromolar zinc applications while NMDA EPSCs from knock-in mice were barely affected (**Fig. 2b**). Hence, the NR2A-H128S mutation ablates high-affinity zinc modulation of NMDARs *in vivo*. Together these data provide unambiguous evidence that NMDARs endogenously expressed in their native synaptic environment are highly sensitive to extracellular zinc, as previously shown in recombinant systems¹⁷.

In contrast to these robust effects on zinc sensitivity, the mutation did not alter expression levels of NR2A, NR2B nor NR1 subunits, or those of AMPA receptors (GluR1), glycine receptors (GlyR α 1) or vesicular zinc transporters (ZnT3, ref²³) in either forebrain and spinal cord (**Fig. 2c, Fig S1 and S2**). Moreover, the NR2B-selective antagonist Ro256981 (1 μ M; ref¹⁴) inhibited knock-in and wild-type hippocampal NMDA EPSCs to the same extent (percentage of inhibition: $47 \pm 2\%$ [n=4] for KI vs $53 \pm 3\%$ [n=3] for WT, P=0.19 Student's *t*-test) revealing that the proportion of synaptic NR2A- vs NR2B-containing NMDA receptors

was unaltered in mutant mice. Similarly, the presence of the NR2A-H128S mutation did not significantly change the synaptic time course of hippocampal NMDA EPSCs (**Fig. S3a**). Furthermore, Timm's staining, which labels chelatable zinc, was identical in brain sections from knock-in and wild-type animals (**Fig. S3b**). Thus, high-affinity zinc modulation of NMDARs is specifically eliminated in NR2A-H128S mice, while the abundance of main excitatory glutamate receptors, the inhibitory glycine receptor (another target of zinc⁷) and synaptic zinc remain unaltered.

Pain responses in NR2A-H128S knock-in mice

We conducted neurological examinations of NR2A-H128S mice. Mutant animals showed a general health comparable to wild-type mice (well-groomed coats and normal body posture, muscle strength, body weight, body temperature, general sensory functions including olfactory, auditory and visual functions, food consumption and locomotor exploration, see **Table S1**). In addition, locomotor habituation in a novel environment and the circadian pattern of locomotor behaviour appeared indistinguishable between mutants and controls (**Fig S4**). Altogether, no major signs of behavioral abnormalities were detected in NR2A-H128S mutant mice.

To investigate whether endogenous Zn²⁺ binding to NR2A subunits is involved in pain control, we examined pain sensitivity in mutant mice (**Fig. 3**). Acute nociception in tail immersion and hot plate tests (**Fig 3a**), as well as tail pressure and Von Frey tests (**Fig 3b**) were unchanged, but mutant mice showed increased responses in response to radiant heat (tail flick and Hargreaves tests) (**Fig 3a**). This hypersensitivity was observed only at heat rates of 0.9 or 2.2 °C/s but not at 4.0 °C/s (**Fig 3c**), revealing a thermal hypersensitivity under slow heat pain stimulation. Mechanisms underlying responses to distinct pain stimuli are complex and recruit multiple primary afferent neurons²⁴. Slow heating conditions (tail flick test at 0.9 or 2.2 °C/s and Hargreaves test) mainly stimulate nociceptive C-fibers whereas fast heating conditions (tail flick test at 4.0 °C/s, tail immersion and hot plate test) preferentially recruit A δ -fibers^{25, 26}. Altogether, these observations suggest that endogenous Zn²⁺ binding to NR2A subunits inhibit C fibers rather than A δ fibers. This is consistent with the notion that excitation of C-fibers, but not A δ -fibers, leads to increased NMDAR function in target spinal cord neurons^{16, 27}.

To further investigate C and A δ fibers involvement, we tested mutant mice for tonic pain responses induced either by capsaicin (a TRPV1 activator that preferentially activates

unmyelinated C-fibers) and TIP 39 (a parathyroid hormone 2 receptor agonist that selectively activates myelinated nociceptive A-fibers)²⁸. NR2A-H128S mice showed clear hypersensitivity to capsaicin, but not to TIP 39 (**Fig. 3d**), indicating that disruption of the Zn²⁺-NR2A interaction enhances C-fiber excitability. Endogenous Zn²⁺ binding to NR2A, therefore, limits NMDAR-regulated excitability mainly at the level of C-fibers.

As NMDA receptors are important actors of chronic pain development^{15,16}, we examined chronic pain responses of NR2A-H128S mice. We used two well-established models of chronic pain, namely Complete Freund's adjuvant-induced (CFA) inflammatory pain and partial sciatic nerve ligation-induced (SNL) neuropathic pain (**Fig 4**). In wild-type mice, both CFA intraplantar administration and SNL induced significant hypersensitivity to heat (heat hyperalgesia in the tail flick test) and tactile stimuli (mechanical allodynia in Von Frey measures). In mutant mice, thermal sensitivity to radiant heat was higher at the basal state under both conditions, as observed in the acute pain experiments. Yet, after CFA and SNL, heat hyperalgesia developed with comparable intensities in both genotypes, and the two groups recovered similarly at day 14 (CFA; **Fig. 4a**) and week 10 (SNL; **Fig. 4b**), suggesting that chronic pain-induced hyperalgesia did not differ between genotypes. In contrast, the amplitude and duration of mechanical allodynia were both strongly increased in mutant animals, and the enhanced mechanical sensitivity of mutant mice was observed in response to both CFA and SNL (**Fig. 4c, 4d**). There was otherwise no change of pain sensitivity at contralateral paws or in sham-control animals in any chronic pain model (**Fig. S5 and S6**). Together, these results demonstrate that the NR2A-H128S mutation specifically increases mechanical allodynia under conditions of persistent pain. Binding of endogenous Zn²⁺ to the NR2A subunit, therefore, reduces mechanical sensitivity as chronic pain develops.

Reasons why Zn²⁺-NR2A binding contributes to reduce chronic pain mainly in the mechanical modality remain to be elucidated. A large body of evidence indicates that NMDARs are over-stimulated under conditions of chronic pain^{15,16}, a phenomenon that influences several signaling pathways²⁹. Future studies will determine the main downstream effectors in the pain-reducing effect of zinc, including for example the well-established nCOX-2 pathway³⁰ known to modulate mechanical sensitivity³¹.

Analgesic effects of exogenous zinc in NR2A-H128S mice

We investigated the analgesic effects of exogenous zinc in wild-type and NR2A-H128S knock-in mouse littermates (**Fig. 5, S7 and S8**). We used the tail flick test, the inflammatory and the neuropathic pain model. Low doses of zinc were administered to avoid

the toxicity associated with high zinc dosage³². Wild-type mice responded strongly to zinc. Indeed, both intrathecal and subcutaneous zinc increased tail withdrawal latency in the tail flick test (**Fig. 5a, b**), in agreement with a previous report³³. Moreover, zinc administration almost completely reversed thermal hyperalgesia and mechanical allodynia in both CFA (**Fig. 5c, d**) and SNL (**Fig. 5e, f**) models of chronic pain. The effect of zinc was observed at a time point where inflammatory and neuropathic pain had fully developed. These results confirm that both local and systemic injections of low-dose zinc produce significant analgesia in rodents³³⁻³⁵ and uncover a remarkably robust effect of zinc under conditions of chronic pain.

In striking contrast, zinc was totally ineffective in NR2A-H128S knock-in mice. Zinc did not modify tail withdrawal responses to acute heat stimulation (**Fig. 5a, b**). Furthermore, neither thermal nor mechanical responses were altered by zinc administration in both inflammatory (**Fig. 5c, d**) and neuropathic (**Fig. 5e, f**) pain models. Overall, the NR2A-H128S mutation abolished all the pain-reducing effects of zinc that were tested. The lack of zinc effects in mutant mice unequivocally demonstrates that high-affinity Zn²⁺ binding to NR2A subunit is essential for zinc-induced analgesia. These results provide a molecular mechanism for the pain-relieving properties of dietary zinc, and strengthen the notion that zinc therapy may successfully treat intractable pain, such as fibromyalgia³⁶, peripheral neuropathy³⁷ or other pain abnormalities³⁸. The zinc phenotype of mutant mice also reveals a largely unanticipated key role of NR2A-containing receptors in pain processing. The involvement of diheteromeric NR1/NR2A receptors containing two copies of the zinc-sensitive NR2A subunit is most probable. In addition, triheteromeric receptors that incorporate both NR2A and non-NR2A subunits and represent a significant fraction of NMDARs^{39, 40} could also contribute, although their zinc sensitivity is lower⁴¹. Currently, there is evidence for the therapeutic utility of NR2B-selective antagonists as analgesics that limit the severe consequences of general NMDAR blockade^{14, 42}. Our finding calls for novel strategies selectively targeting zinc-sensitive NR2A-containing receptors for controlling persistent pain states.

CONCLUSION

In conclusion, the remarkable pain phenotype observed in knock-in NR2A-H128S mice demonstrates that high-affinity Zn²⁺ binding to the NR2A subunit is sufficient to dampen NMDAR function in pain pathways. Since the NR2A-H128S mutation eliminates sensitivity of NMDARs to nanomolar -but not micromolar- zinc concentrations¹⁸⁻²⁰, our data strongly suggest that extracellular zinc levels that fine-tune NMDAR activity *in vivo* are in the

submicromolar range. Endogenous zinc, therefore, regulates NMDAR function at concentrations far lower than previous estimations^{2,3}. The origin of zinc diffusing in the vicinity of NMDARs is yet to be determined. Zn²⁺ ions co-stored with glutamate in synaptic vesicles and released during neuronal activity are obvious candidates²³. Inhibitory GABAergic neurons, which in the spinal cord form a major contingent of zinc-containing terminals⁴³, may provide additional sources of zinc. Finally, NMDA-dependent spinal LTP is well recognized as a cellular substrate for hyperalgesia⁴⁴, and is blocked by exogenous zinc⁴. Future experiments using NR2A-H128S mutant mice will determine the role of endogenous zinc acting at NR2A subunits in spinal plasticity. Altogether, our data reveal that high-affinity Zn²⁺ binding to the NR2A subunit is a fundamental molecular event in major aspects of pain transmission, chronic pain development and zinc-induced analgesia. This discovery has important implications for pain physiopathology, and its management in the clinic.

METHODS

Methods and any associated references are available in the online version of the paper at <http://www.nature.com/natureneuroscience/>.

ACKNOWLEDGEMENTS

We thank Blandine Puvion, Audrey Matifas and Rafael Weibel for technical assistance and Eric Krejci for help with the targeting vector. This research was supported by the CNRS, INSERM, the Université de Strasbourg, the French ANR grant SynapticZinc (P.P and B.K.), the US NIH NIDA grant #DA05010 (B.K.) and an “Equipe FRM” grant (P.P.). C.N. was supported by the Fondation pour la Recherche Médicale (FRM) and A.M.V. by the Région Ile-de-France. We thank Boris Barbour, Jérôme Becker and Eric Schwartz for comments on the manuscript.

AUTHOR CONTRIBUTIONS

BLK and PP designed and supervised the study. DF, JN and ALG contributed to the creation NR2A-H128S mutant mouse line. JN and PP performed the electrophysiological experiments on Xenopus oocytes. AMV ran electrophysiological characterization of mutant mice and performed the Timm’s staining. CN performed all the pain experiments. DR and AO conducted neurological examination of mutant mice. SC and AMV performed immunochemistry. CG and JN contributed to conceptual aspects of the study. CN, AMV, CG, AO, PP and BLK wrote the manuscript.

COMPETING FINANCIAL INTERESTS

The authors declare no competing financial interest

1. Hambidge, K.M. & Krebs, N.F. Zinc deficiency: a special challenge. *J Nutr* **137**, 1101-1105 (2007).
2. Frederickson, C.J., Suh, S.W., Silva, D. & Thompson, R.B. Importance of zinc in the central nervous system: the zinc-containing neuron. *J Nutr* **130**, 1471S-1483S (2000).
3. Vogt, K., Mellor, J., Tong, G. & Nicoll, R. The actions of synaptically released zinc at hippocampal mossy fiber synapses. *Neuron* **26**, 187-196 (2000).
4. Ma, J.Y. & Zhao, Z.Q. The effects of Zn²⁺ on long-term potentiation of C fiber-evoked potentials in the rat spinal dorsal horn. *Brain Res Bull* **56**, 575-579 (2001).
5. Ueno, S., *et al.* Mossy fiber Zn²⁺ spillover modulates heterosynaptic N-methyl-D-aspartate receptor activity in hippocampal CA3 circuits. *J Cell Biol* **158**, 215-220 (2002).
6. Kodirov, S.A., *et al.* Synaptically released zinc gates long-term potentiation in fear conditioning pathways. *Proc Natl Acad Sci U S A* **103**, 15218-15223 (2006).
7. Hirzel, K., *et al.* Hyperekplexia phenotype of glycine receptor alpha1 subunit mutant mice identifies Zn(2+) as an essential endogenous modulator of glycinergic neurotransmission. *Neuron* **52**, 679-690 (2006).
8. Sensi, S.L., Paoletti, P., Bush, A.I. & Sekler, I. Zinc in the physiology and pathology of the CNS. *Nat Rev Neurosci* **10**, 780-791 (2009).
9. Velazquez, R.A., Cai, Y., Shi, Q. & Larson, A.A. The distribution of zinc selenite and expression of metallothionein-III mRNA in the spinal cord and dorsal root ganglia of the rat suggest a role for zinc in sensory transmission. *J Neurosci* **19**, 2288-2300 (1999).
10. Jo, S.M., Danscher, G., Schroder, H.D. & Suh, S.W. Depletion of vesicular zinc in dorsal horn of spinal cord causes increased neuropathic pain in mice. *Biometals* **21**, 151-158 (2008).
11. Smart, T.G., Hosie, A.M. & Miller, P.S. Zn²⁺ ions: modulators of excitatory and inhibitory synaptic activity. *Neuroscientist* **10**, 432-442 (2004).
12. Frederickson, C.J., Koh, J.Y. & Bush, A.I. The neurobiology of zinc in health and disease. *Nat Rev Neurosci* **6**, 449-462 (2005).
13. Paoletti, P., Vergnano, A.M., Barbour, B. & Casado, M. Zinc at glutamatergic synapses. *Neuroscience* **158**, 126-136 (2009).
14. Traynelis, S.F., *et al.* Glutamate receptor ion channels: structure, regulation, and function. *Pharmacol Rev* **62**, 405-496 (2010).
15. Woolf, C.J. & Salter, M.W. Neuronal plasticity: increasing the gain in pain. *Science* **288**, 1765-1769 (2000).
16. Latremoliere, A. & Woolf, C.J. Central sensitization: a generator of pain hypersensitivity by central neural plasticity. *J Pain* **10**, 895-926 (2009).
17. Paoletti, P., Ascher, P. & Neyton, J. High-affinity zinc inhibition of NMDA NR1-NR2A receptors. *J Neurosci* **17**, 5711-5725 (1997).
18. Paoletti, P., *et al.* Molecular organization of a zinc binding n-terminal modulatory domain in a NMDA receptor subunit. *Neuron* **28**, 911-925 (2000).
19. Fayyazuddin, A., Villarroel, A., Le Goff, A., Lerma, J. & Neyton, J. Four residues of the extracellular N-terminal domain of the NR2A subunit control high-affinity Zn²⁺ binding to NMDA receptors. *Neuron* **25**, 683-694 (2000).

20. Low, C.M., Zheng, F., Lyuboslavsky, P. & Traynelis, S.F. Molecular determinants of coordinated proton and zinc inhibition of N-methyl-D-aspartate NR1/NR2A receptors. *Proc Natl Acad Sci U S A* **97**, 11062-11067 (2000).
21. Gielen, M., Sieglér Retchless, B., Mony, L., Johnson, J.W. & Paoletti, P. Mechanism of differential control of NMDA receptor activity by NR2 subunits. *Nature* **459**, 703-707 (2009).
22. Scherrer, G., *et al.* Knockin mice expressing fluorescent delta-opioid receptors uncover G protein-coupled receptor dynamics in vivo. *Proc Natl Acad Sci U S A* **103**, 9691-9696 (2006).
23. Cole, T.B., Wenzel, H.J., Kafer, K.E., Schwartzkroin, P.A. & Palmiter, R.D. Elimination of zinc from synaptic vesicles in the intact mouse brain by disruption of the ZnT3 gene. *Proc Natl Acad Sci U S A* **96**, 1716-1721 (1999).
24. Basbaum, A.I., Bautista, D.M., Scherrer, G. & Julius, D. Cellular and molecular mechanisms of pain. *Cell* **139**, 267-284 (2009).
25. Yeomans, D.C., Pirec, V. & Proudfit, H.K. Nociceptive responses to high and low rates of noxious cutaneous heating are mediated by different nociceptors in the rat: behavioral evidence. *Pain* **68**, 133-140 (1996).
26. Le Bars, D., Gozariu, M. & Cadden, S.W. Animal models of nociception. *Pharmacol Rev* **53**, 597-652 (2001).
27. Drdla, R. & Sandkuhler, J. Long-term potentiation at C-fibre synapses by low-level presynaptic activity in vivo. *Mol Pain* **4**, 18 (2008).
28. Matsumoto, M., Kondo, S., Usdin, T.B. & Ueda, H. Parathyroid hormone 2 receptor is a functional marker of nociceptive myelinated fibers responsible for neuropathic pain. *J Neurochem* **112**, 521-530 (2010).
29. Svensson, C.I., Hua, X.Y., Protter, A.A., Powell, H.C. & Yaksh, T.L. Spinal p38 MAP kinase is necessary for NMDA-induced spinal PGE(2) release and thermal hyperalgesia. *Neuroreport* **14**, 1153-1157 (2003).
30. Yaksh, T.L., Hua, X.Y., Kalcheva, I., Nozaki-Taguchi, N. & Marsala, M. The spinal biology in humans and animals of pain states generated by persistent small afferent input. *Proc Natl Acad Sci U S A* **96**, 7680-7686 (1999).
31. Vardeh, D., *et al.* COX2 in CNS neural cells mediates mechanical inflammatory pain hypersensitivity in mice. *J Clin Invest* **119**, 287-294 (2009).
32. Hu, H., Bandell, M., Petrus, M.J., Zhu, M.X. & Patapoutian, A. Zinc activates damage-sensing TRPA1 ion channels. *Nat Chem Biol* **5**, 183-190 (2009).
33. Larson, A.A. & Kitto, K.F. Manipulations of zinc in the spinal cord, by intrathecal injection of zinc chloride, disodium-calcium-EDTA, or dipicolinic acid, alter nociceptive activity in mice. *J Pharmacol Exp Ther* **282**, 1319-1325 (1997).
34. Safieh-Garabedian, B., *et al.* Zinc reduces the hyperalgesia and upregulation of NGF and IL-1 beta produced by peripheral inflammation in the rat. *Neuropharmacology* **35**, 599-603 (1996).
35. Liu, T., Walker, J.S. & Tracey, D.J. Zinc alleviates thermal hyperalgesia due to partial nerve injury. *Neuroreport* **10**, 1619-1623 (1999).
36. Sendur, O.F., Tastaban, E., Turan, Y. & Ulman, C. The relationship between serum trace element levels and clinical parameters in patients with fibromyalgia. *Rheumatol Int* **28**, 1117-1121 (2008).
37. Head, K.A. Peripheral neuropathy: pathogenic mechanisms and alternative therapies. *Altern Med Rev* **11**, 294-329 (2006).
38. Yoshida, H., Tsuji, K., Sakata, T., Nakagawa, A. & Morita, S. Clinical study of tongue pain: Serum zinc, vitamin B12, folic acid, and copper concentrations, and systemic disease. *Br J Oral Maxillofac Surg* (2010).

39. Al-Hallaq, R.A., Conrads, T.P., Veenstra, T.D. & Wenthold, R.J. NMDA di-heteromeric receptor populations and associated proteins in rat hippocampus. *J Neurosci* **27**, 8334-8343 (2007).
40. Rauner, C. & Kohr, G. Triheteromeric NR1/NR2A/NR2B receptors constitute the major N-methyl-D-aspartate (NMDA) receptor population in adult hippocampal synapses. *J Biol Chem* (2010).
41. Hatton, C.J. & Paoletti, P. Modulation of triheteromeric NMDA receptors by N-terminal domain ligands. *Neuron* **46**, 261-274 (2005).
42. Mony, L., Kew, J.N., Gunthorpe, M.J. & Paoletti, P. Allosteric modulators of NR2B-containing NMDA receptors: molecular mechanisms and therapeutic potential. *Br J Pharmacol* **157**, 1301-1317 (2009).
43. Danscher, G., *et al.* Inhibitory zinc-enriched terminals in mouse spinal cord. *Neuroscience* **105**, 941-947 (2001).
44. Sandkuhler, J. Understanding LTP in pain pathways. *Mol Pain* **3**, 9 (2007).

Figure Legends

Fig. 1. Targeting the NMDA receptor NR2A subunit gene in mice.

(a) The NR2A-H128S mutant allele was created by homologous recombination. The scheme shows the wild type *NR2A* allele, the targeting vector, the targeted allele and the H128S knock-in allele. The CAT codon encoding histidine (H) 128 in exon 1 was replaced by the TCC codon encoding serine (S), and a floxed neo cassette was introduced 3' from exon 1 to select for ES cells harboring the knock-in allele. The final mutant allele was obtained after excision of the Neo-cassette by a Cre recombinase treatment of ES cells. White box, exon 1; star in white box shows the H128S mutation; dark line, intronic sequences; Ba, BamHI; Bs, Bsu361 restriction sites; triangles, *loxP* sites; Neo box, neomycin-resistance cassette; grey bars, probes for Southern blot analysis; lines above gene indicate expected labeled DNA fragments in Southern blot analysis. (b) Southern blot analysis of wild-type and targeted alleles in the selected ES clone. Genomic DNA was digested with Bsu 361 and BamHI, and hybridized with 5' and 3' external probes, respectively, or the neo probe. Expected bands at each size are obtained, as indicated on panel A. (c) Genomic DNA sequence analysis using tail biopsies from wild-type (left panel) and knock-in homozygous mutant (right panel) animals, showing the replacement of the the CAT codon by the mutated TCC codon. (d) Genotyping of the NR2A-H128S knock-in line. PCR analysis using mutation-specific primers (strategy on left) reveals wild-type (280 bp) and mutant (315 bp) alleles (right). White arrow, forward primer for WT DNA, black arrow, forward primer for mutant DNA, grey arrow, reverse primer. Analysis of genomic DNA from wild-type NR2A, homozygous NR2A-H128S and heterozygous NR2A WT/NR2A-H128S animals is shown. The 35 bp differences between mutant and wild-type alleles results from the remaining lox P site in the mutant allele.

Fig. 2. High-affinity zinc inhibition of NMDA currents is lost in NR2A-H128S mice. (a)

Sensitivity to subunit-specific modulators of brain NMDARs from wild-type (WT) and knock-in NR2A-H128S (KI) mice transplanted into *Xenopus* oocytes. Inhibition by 20 nM zinc was abolished in KI mice (upper traces; 2.3 ± 1.3 %, $n=6$ vs 30.3 ± 4.2 % $n=10$ for WT; mean \pm SD, *** $P < 0.001$, Student's *t*-test), while inhibition by the NR2B-selective antagonist ifenprodil was unchanged (lower traces; 25.2 ± 3.2 %, $n=6$ vs 24.8 ± 2.4 % $n=13$ for WT; $P=0.7$). NMDA currents were induced by co-application of 300 μ M NMDA, 100 μ M glycine and 10 μ M strychnine (N+G+S). (b) Hippocampal Schaeffer-collateral/CA1 NMDA EPSCs from KI mice were insensitive to 300 nM zinc contrasting with the marked inhibition seen on

WT mice (peak current ratio: 0.48 ± 0.03 $n=4$ vs 0.93 ± 0.06 $n=5$ for KI; *** $P<0.001$, Student's *t*-test). *Idem* for NMDA EPSCs recorded in the dorsal horn of the spinal cord (0.59 ± 0.05 , $n=6$ for WT vs 1.03 ± 0.07 , $n=6$ for KI; *** $P<0.001$). (c) Unaltered protein expression levels in KI mice compared to WT mice in forebrain (top) and spinal cord (bottom). Lower band, α -tubulin control (α -tub). Full-length blots are presented in Supplementary Figure S1. For each protein, quantification was performed on 2 or 3 different WT/KI couples; no significant changes in expression level was detected ($P>0.05$ one-sample Student's *t*-test; see Supplementary Figure S2).

Fig. 3. NR2A-H128S mice show enhanced basal pain sensitivity in response to radiant heat and capsaicin. Tail immersion (TI), hot plate (HP), tail flick (TF), Hargreaves (HT), von Frey filaments (VF), tail pressure (TP) and chemical tests by capsaicin (CAP) and TIP39 (TIP) were used to evaluate basal pain sensitivity in response to thermal (a, c), mechanical (b) and chemical (d) noxious stimuli (see Methods). No genotype effect was observed in TI withdrawal at three temperatures (a, top), in the HP response (a, bottom), in the mechanical responses (b), or in the TIP response (d, top). In contrast, significant hypersensitivity of NR2A-H128 mice was detected in responses to radiant heat stimuli (a, bottom) and capsaicin (d, CAP; kinetics shown at bottom). Furthermore, tail flick test with three different heat rates showed thermal hypersensitivity at 0.9 and 2.2 °C/s (c). Data are expressed as means \pm SEM of 8 mice/group. Significance is indicated by $\star P<0.05$ and $\star\star\star P<0.001$, NR2A-H128S mutants vs controls, Student's *t*-test.

Fig. 4. NR2A-H128S mice show increased mechanical allodynia under chronic pain. Thermal and mechanical sensitivity of mutant mice (KI) and their controls (WT) was examined under CFA inflammatory or SNL neuropathic pain. Raw values (left) and percent pain (right) are shown. Dotted line, base-line value. (a, b) Thermal sensitivity (Hargreaves test). Areas under the curve (AUC) of percent pain show no genotype difference in intensity and duration of thermal hyperalgesia under both CFA (a) and SNL (b) conditions (not shown). (c, d) Mechanical sensitivity (von-Frey test). Upon CFA injection (c), as well as after partial sciatic nerve ligation (d), mechanical allodynia developed with higher intensity and duration in mutant mice (AUC value of percent pain: CFA: 316 ± 15 , WT mice vs. 510 ± 7.3 , KI mice; SNL: 565 ± 12 , WT mice vs. 778 ± 14 , KI mice). Data are expressed as means \pm SEM of 8 mice/group. Significance is indicated by $\star P<0.05$, $\star\star P<0.01$ and $\star\star\star P<0.001$, NR2A-H128S mutants vs controls for individual time points, Student's *t*-test.

Fig. 5. Zinc analgesia is abolished in NR2A-H128S mice. Zinc analgesia was examined in mutant (KI) and control (WT) mice after i.t. (0.2 nmol, left panels) or s.c. (0.1-1 mg/kg, right panels) ZnCl₂ administration. Baseline thresholds (BL) were measured in naive mice before the drug injection or induction of chronic pain. **(a, b)** Acute thermal pain (tail flick test. Raw values (left panels) and %MPE (right panels) show zinc analgesia in wild-type but not mutant mice. Data are expressed as means ± SEM of 8 mice/group. Significance is indicated by ★P<0.05, ★★P<0.01 and ★★★P<0.001, zinc-treated group vs saline-treated group for individual time points, Student's *t*-test. **(c, d)** CFA inflammatory pain. Both i.t. or s.c. zinc administrations inhibited CFA-induced thermal hyperalgesia (Hargreaves test, left panels) and mechanical allodynia (von Frey test, right panels). These antihyperalgesic and antiallodynic effects were absent in mutant mice. **(e, f)** SNL neuropathic pain. As for inflammatory pain, both i.t. or s.c. zinc inhibited thermal hyperalgesia (Hargreaves test, left panels) and mechanical allodynia (von Frey test, right panels) induced by nerve ligation. These antihyperalgesic and antiallodynic effects were absent in mutant mice. For both CFA and SNL experimental series, data are expressed as means ± SEM of 8 mice/group. Significance is indicated by ★★★P<0.001 for zinc-treated vs saline-treated groups and ☆☆☆P<0.001 for mutants vs controls, two-way repeated measures ANOVA followed by Bonferroni-Dunn test.

ONLINE METHODS

Animal procedures.

All experiments were performed in accordance with the European Communities Council Directive of 24 November 1986. Mice were housed in temperature- and humidity-controlled animal colony on a 12 h dark-light cycle with food and water *ad libitum*. For behavioral studies, mice were around 12 weeks-old. Researchers were blind to genotype and treatment during behavioral experiment. All data are presented as means \pm SEM.

Generation of NR2A-H128S knock-in mice.

We generated mice carrying the H128S mutation in the NR2A subunit (see **Fig. 1a**). An 11-kb genomic clone containing exon-1 of *NR2A* gene (NM_008170 05-APR-2010) was isolated from C57Bl/6 mouse genomic DNA and cloned into pUC18. This clone was engineered to introduce the H to S mutation (CAT to TCC) at position 128, a floxed-Neo cassette at 3' side and a thymidine-kinase/DTA-coding cassette at 5' side. The targeting vector was linearized and electroporated into 129/SV derived embryonic stem (ES) cells followed by neomycin selection. Selected colonies were screened for homologous recombination by Southern blotting with either Bsu361 or BamHI digests, using 5' and 3' external probes or Neo probe (see **Fig. 1a, b**). Neo-cassette insertion was screened by long-range PCR. A positive clone was transfected with a Cre recombinase-expressing plasmid to remove the floxed-Neo cassette, which was verified by PCR. ES cells with correct genotype were injected into C57BL/6 blastocysts, and resulting chimeric males were bred with C57BL/6 females for germline transmission. Heterozygous NR2A^{H128S/+} mice were crossed to generate the homozygous NR2A^{H128S/H128S} mouse line, referred as to NR2A-H128S throughout the study. To confirm the NR2A-H128S mutation, genomic DNA from mutated mice was PCR-amplified and confirmed by DNA sequencing (**Fig. 1c**). Genotyping of NR2A-H128S mutant mice was performed as for ES cell screening. The 35 bp difference between knock-in (KI) and wild-type (WT) alleles resulted from the remaining loxP site in the KI allele. Forward primers used were 5'TCATCCCCATCTTGGGCATTCAT3' for WT-DNA, 5'TCATCCCCATCTTGGGCATTTCC3' for KI-DNA and reverse primer was 5'AGCATCTGAGTACCCCATCTTCAA3' (**Fig. 1d**). All experimental mice (WT and KI) were on a 50 % C57BL/6J – 50 % 129/SV genetic background and were littermates obtained by crossing heterozygous breeders NR2A^{H128S/+}.

Transplantation of mouse brain membranes into *Xenopus laevis* oocytes and measurements of NMDA currents

Forebrain membranes were prepared and injected in *Xenopus laevis* oocytes following the protocol adapted from ref⁴⁵. Briefly: using a Teflon glass homogenizer, ~0.5 g of forebrain from 5-week old mice was homogenized in 4 ml glycine buffer A (in mM: 200 glycine, 150 NaCl, 50 EGTA, 50 EDTA, 300 sucrose, pH 9.0 with NaOH) plus protease inhibitors (1/1000 pepstatin, 1/1000 leupeptin and 3x 20 µl PMSF 150 mM). The homogenate was centrifuged at 9,500 g for 10 min (room temperature). The supernatant was centrifuged for 2 h at 130,000 g (4 °C). The pellet was washed with 4 ml glycine buffer B (in mM: 5 glycine, 1 EDTA, pH 7.5 with NaOH), resuspended in 200 µl glycine buffer B, aliquoted in 10 µl vials that were quickly frozen on dry-ice and kept at -80 °C. Immediately prior use, membrane samples were thawed and directly injected into defolliculated oocytes (~50 nl/oocyte; ~10 mg protein/ml). One or two days after injection, NMDA currents were recorded (-60 mV) by applying saturating concentrations of NMDA (300 µM) and glycine (100 µM) to the extracellular perfusion solution. Strychnine (10 µM) was also added to avoid inhibitory glycine receptor activation. Oocytes preparation, injection, voltage-clamping and superfusion are previously described^{18, 19}. In zinc sensitivity experiments, tricine (N-tris[hydroxymethyl]methylglycine, 10 mM) was used to buffer zinc¹⁷ following the relationship^{17, 19}: $[Zn]_{\text{free}} = [Zn]_{\text{added}}/200$. In ifenprodil sensitivity experiments, DTPA (10 µM) was added to chelate trace amounts of heavy metals¹⁷. Recordings were performed at room temperature.

Patch-clamp recordings of synaptic NMDA currents.

Hippocampal slice preparation. Acute horizontal hippocampal slices were prepared from 3-4 weeks-old mice. Mice were anesthetized with sodium pentobarbital (30 mg/kg), decapitated and brains were placed in ice-cold ACSF containing (in mM): 125 NaCl, 26 NaHCO₃, 2.5 KCl, 1.25 NaH₂PO₄, 2 CaCl₂, 1 MgCl₂, 20 glucose bubbled with 95% O₂-5% CO₂. Slices (320 µm thick) were cut in ice-cold ACSF supplemented with 50 µM D-APV

Spinal cord slice preparation. Under sodium pentobarbital anaesthesia, 3-weeks-old mice were decapitated and spinal cord was removed by hydraulic extrusion. Transverse slices (290 µm thick) were cut mainly from the lumbar segment in ice-cold solution (in mM: 130 K-gluconate, 15 KCl, 0.2 EGTA, 20 HEPES, 25 glucose, pH 7.4 with NaOH) supplemented with 50 µM D-APV, 0.5 µM TTX and 50 nM minocycline.

Recording conditions, data acquisition and analysis. Slices were transferred to a recording chamber perfused with bubbled ACSF and visualized in the transmitted deep red light (~750 nm) using a CoolSnap CF CCD camera (Photometrics, Trenton, NJ).

Patch pipettes were filled with intracellular solution containing (in mM): 125 Cs-gluconate, 20 BAPTA, 5 QX-314, 5 TEA-Cl, 10 HEPES, 4 ATP-Mg and 0.2 GTP-Na; pH 7.3 with CsOH. Pipette resistance was in the range 4-8 M Ω .

For hippocampal recordings, whole-cell voltage-clamp recordings of excitatory postsynaptic NMDA receptor mediated currents (NMDA EPSCs) were obtained from CA1 pyramidal cells by stimulating the Schaeffer collateral input in presence of tricine (10 mM), NBQX (10 μ M) and bicuculline (10 μ M). To avoid antidromic CA3 stimulation, we cut between CA3 and CA1 regions. For spinal cord recordings, NMDA EPSCs were obtained from dorsal horn lamina II cells by focal stimulation of the tissue in a perimeter of 50-100 μ m around the patched cell. Lamina II cells were recorded in presence of tricine (10 mM), NBQX (10 μ M), bicuculline (10 μ M), strychnine (1 μ M) and RO-256981 (1 μ M) to minimize the contribution of putative presynaptic NR2B-containing NMDA receptors^{46, 47}. Cells were held at +40 mV. Stimulation pipettes were filled with HEPES-buffered solution and stimulation pulses were provided at 0.1 Hz. Intensities of stimuli ranged from 0.4 to 8 mA, durations were 0.1 ms and 0.3 ms for hippocampal and dorsal horn recordings, respectively. Zinc was buffered using 10 mM tricine (see above).

Recordings were performed at 35 °C (hippocampal slices) or 26 °C (spinal cord slices) using EPC-10 amplifier run with Patch Master software (HeKa Elektronik, Lambrecht/Pfalz, Germany). Data were acquired at 10 or 20 kHz and filtered at 3 kHz. Series resistance was monitored regularly during recording and compensated at 60-70 %. Data were analyzed using NeuroMatic (<http://www.neuromatic.thinkrandom.com>) within the IGOR-Pro environment (WaveMetrics, Lake Oswego, OR). Student's *t*-test was used for statistical comparisons.

Western Blots.

3-months-old animals were anaesthetized with sodium pentobarbital and decapitated. Forebrains were dissected in ice-cold Mg-ACSF-similar composition (ACSF with CaCl₂ and MgCl₂ concentrations swapped). Thoracic and lumbar portions of spinal cords were rapidly removed by hydraulic extrusion in Mg-ACSF. Isolated forebrains and spinal cords are homogenated with a Teflon glass homogenizer in 500 μ l buffer 1 (in mM: 320 sucrose, 5 HEPES pH 7.4, plus a protease inhibitor cocktail tablet (Complete, Mini, Roche)). After 200 μ l buffer 1 addition, cells nuclei and debris were removed by centrifugation twice at 1,000 g

for 10 min, 4 °C. Enriched membrane fractions were collected by supernatant centrifugation at 100,000 g for 30 min, 4 °C. Pellets were re-suspended in 500 µl buffer 2 (5 mM Tris-HCl pH 8.1, 0.5% Triton X-100, plus protease inhibitors). Preparations were used immediately for immuno-detection experiments or stored at -80°C.

Mice forebrains and spinal cord samples were separated in non-reducing conditions by 4-12 % SDS-PAGE, dry-transferred to nitrocellulose membrane and immuno-blotted with the following antibodies: anti-NR1 (1:1000, mouse monoclonal Ab clone 54.1, Millipore); anti-NR2B (1:100, mouse monoclonal Ab clone 13, BD Transduction); anti-NR2A (1:500, rabbit monoclonal Ab clone A12W, Millipore); anti-GluR1 (1:300, rabbit polyclonal Ab, Millipore); anti-ZnT3 (1:100, kindly provided by Victor Faundez, Emory University, Atlanta); anti-GlyR α 1 (1:1000, monoclonal mouse antibody Ab 4a, Synaptic Systems) and anti- α -Tubulin (1:5000, mouse monoclonal Ab clone DM1A, Millipore) to normalize proteins signals. Proteins bands were visualized using secondary peroxidase-linked goat anti-rabbit or anti-mouse antibodies (1:10000, Jackson ImmunoResearch), with the SuperSignal® West Pico Chemiluminescent Substrate (Thermo Scientific).

Western blot quantification was performed using the NIH ImageJ software. For each protein and given WT/KI mouse couple, band intensities between WT and KI samples were compared and normalized to the intensity ratio between respective α -tubulin signals (protein ratio (KI/WT) = [protKI/protWT] x [tubWT/tubKI]). This procedure was repeated several times using different couples and mean protein ratio (KI/WT) was calculated. Statistics were performed using one-sample Student's t-test.

Timm's staining.

3-weeks or 3-months-old mice were anaesthetized with 7 % chloral hydrate and intracardially perfused with the following successive solutions: 0.9% NaCl, Timm Solution (in mM: 24 Na₂S-9H₂O, 43 NaH₂PO₄) and finally 4% paraformaldehyde in 0.1 M phosphate buffer (PFA-PB; pH 7.2) at ~4 °C. Brains were dissected and post-fixed in PFA-PB overnight at 4 °C and cut in 50 µm thick coronal slices with vibratome in cold PBS (Euromedex, France). Sections were rehydrated, mounted on gelatine coated slides, and developed for 45 min in the dark at room temperature in a solution comprising: 60 ml 50 % arabic gum, 10 ml 2 M citrate buffer, 30 ml 0.5 M hydroquinone and 1 ml 1 M silver nitrate. After rinsing, slide was placed in 30 % sodium thiosulfate solution, rinsed again in ddH₂O, dehydrated and finally coverslipped.

Neurological examinations.

General health of mice was evaluated by measuring body weight, body temperature and overt behavioral signs (coat appearance, body posture, secretory signs).

Sensory functions were evaluated using the following score: 0: no response, 1: response.

Visual ability: Orientation responses to a moving object (cotton swab) in each peripheral visual field at a distance of 5 cm were assessed.

Audition: Preyer and startle reflexes (pinna flicking backwards, startle) to 90 dB click noise of 20 kHz frequency and acoustic startle was tested.

Olfaction: Olfactory exploration of an object (cotton swab) presented in front of the animal's muzzle was examined.

Tactile perception: Evaluated by reaction to pinna and corneal touch using a cotton wire.

Motor functions were evaluated as follows:

Rotarod test: Mice were submitted to 3 testing trials separated by 5-10 min interval and during the speed rotation accelerates from 4 to 40 rpm in 5 min (Bioseb, Chaville, France).

The falling latency was recorded.

String test: The apparatus was a wire stretched horizontally 40 cm above a table. Testing consisted of 3 consecutive trials separated by 5-min interval. On each trial the animal forepaws were placed on the wire and falling latency was recorded with 60 sec cut-off.

Grip test: The maximal muscle strength was measured using isometric dynamometer connected to a grid (Bioseb, Chaville, France). Once the animal gripped the grid with its forepaws, it was slowly pulled back until released. The maximal strength developed was recorded; results are given in gram per body weight (g/g).

Locomotor activity and rearing: Mice were tested in automated open fields (Panlab, Barcelona, Spain). The open fields were placed in homogeneously illuminated room (150 Lux). Each mouse was placed in the periphery of open field and allowed to explore freely for 30 min. The distance traveled and the rearing number was recorded over the test session.

Locomotor habituation, circadian activity and food consumption.

Spontaneous locomotor activity and food consumption were measured in the electronic monitoring system (Imetronic, Pessac, France). Each testing box composed of detachable cage is equipped with food magazine, drinking bottle, infra-red captors to measure ambulatory locomotor activity and rears. Food consumption is recorded as number of 20 mg pellets delivered during the testing by an automated pellet feeder. Mice were placed in the

boxes at 11:00 for a 32 h period in order to measure habituation (first 5 testing hours) as well as nocturnal and diurnal activities. The light in the boxes was on from 7:00 to 19:00 and switched off automatically from 19:00 to 7:00, which is exactly same light/dark cycle as in the holding room.

Nociceptive thresholds.

Experiments were performed between 9:00-15:00 and animals were habituated to the testing area for 20 minutes. For tail immersion, tail flick and tail pressure test, each mouse was lightly restrained in 50 ml cylinder and habituated twice daily for 3 days.

Tail immersion and tail flick test: Tail immersion test was conducted by immersing the tail (5 cm from the tip) into water bath at 46°C, 48°C and 50°C⁴⁸. Tail flick test was conducted by exposing the tail to radiant heat (Bioseb, Valbonne, France). For both test, tail withdrawal latencies were determined with cut-off of 30 s. To examine the heat rate-depend hypersensitivity on tail flick test, heat intensity of 10 (0.9 °C/s), 20 (2.2 °C/s) and 50 (4.0 °C/s) on heat source was used. To evaluate zinc-induced analgesia, maximum possible effect (%MPE) was calculated by following equation: $\%MPE = (\text{latency}_{\text{zinc}} - \text{latency}_{\text{baseline}}) / (30 - \text{latency}_{\text{baseline}})$

Hargreaves test: The radiant heat source (Bioseb, Valbonne, France) was focused on plantar surface of the hindpaw⁴⁸. The paw withdrawal latency was measured automatically with cut-off of 30 s.

Hot plate test: Latency for hindpaw discomfort (jumping, licking and shaking) after putting mice on 52°C hot plate (Bioseb, Valbonne, France) was measured (cut-off: 120 s)⁴⁸.

Tail pressure test: Gradual increasing pressure by the pressure stimulation unit with conic tip (Bioseb, Valbonne, France) was applied to tail⁴⁸. Pressure threshold of tail withdrawal were determined with 500 g cut-off value.

Von-Frey test: A series of eight von-Frey filaments (bending force: 0.008-2 g) was applied to the hindpaw according to the up-and-down method⁴⁸. Response threshold was calculated by the Excel program generously provided from Alan Basbaum's laboratory (UCSF, CA, USA).

Inflammatory pain.

Inflammatory pain was induced by intraplantar injection of Complete Freund's adjuvant (CFA) to left hindpaw⁴⁸. Response to heat (day 1-14) and mechanical (day 1-24) stimuli was assessed after injection of 4 µl CFA (**Fig 3**). For zinc analgesia, pain measurement was performed 2 or 3 days after injection of 8 µl CFA for both heat and

mechanical responses (**Fig. 4**). Pain sensitivity was evaluated by raw value or percentage pain value calculated by; $\text{percentage pain} = (\text{Value}_{\text{contra}} - \text{Value}_{\text{ipsi}}) / (\text{Value}_{\text{contra}})$.

Neuropathic pain.

Neuropathic pain model mice were produced by ligating left sciatic nerve according to the method previously described⁴⁸. Sham mice were produced by same surgery without nerve ligation. Response to heat (week 1-10) and mechanical (week 1-12) stimuli was assessed after the surgery (**Fig 3**). For zinc analgesia, pain measurement was performed on week 2-3 for both heat and mechanical responses (**Fig. 4**). Pain sensitivity was evaluated by raw value or percentage pain value as described above.

Chemical pain.

Intraplantar injection of molecules that stimulate preferably C fibers (capsaicin⁴⁹) or A δ fibers (TIP39²⁸) was used to assess chemical pain. Mice were habituated in Plexiglas cage for 30 min before testing. Capsaicin (1.6 $\mu\text{g}/10 \mu\text{l}$) or TIP39 (100 pmol/10 μl) was injected into the plantar surface of right hind paw. Duration of nociceptive responses (licking, biting and shaking) was recorded for 10 min.

Zinc administration.

Zinc chloride was dissolved in 0.9% saline and injected intrathecally or subcutaneously. To examine the zinc antinociception, zinc solution was injected 30 min before the first measurement and effect was measured each 30 min until 240 min after injection. To examine the zinc antihyperalgesia and antiallodynia, zinc solution was injected 90 min before the testing.

Chemicals and drugs.

2,3-dihydroxy-6-nitro-7-sulfamoyl-benzo[f]quinoxaline-2,3-dione (NBQX), bicuculline methochloride, D-(-)-2-amino-5-phosphonovaleric acid (D-APV), QX-314 and tetrodotoxin (TTX) were from Ascent Scientific (Bristol, UK). Mouse TIP39 was from Phoenix Pharmaceuticals (Burlingame, CA, USA). Zinc chloride and all other compounds were from Sigma (St Louis, MO, USA). Ifenprodil and Ro 25-6981 were generous gift from Sanofi-Synthelabo (Bagneux, France) and Hoffmann-La-Roche (Basel, Switzerland), respectively.

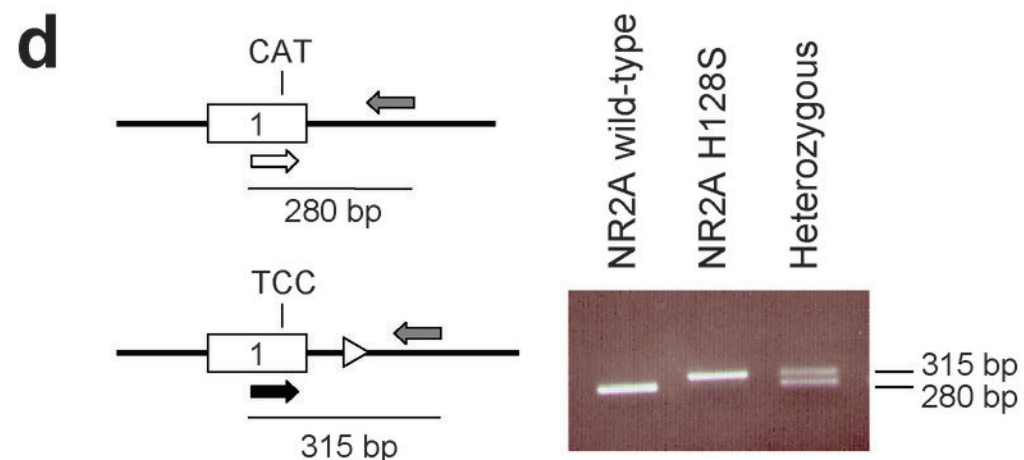
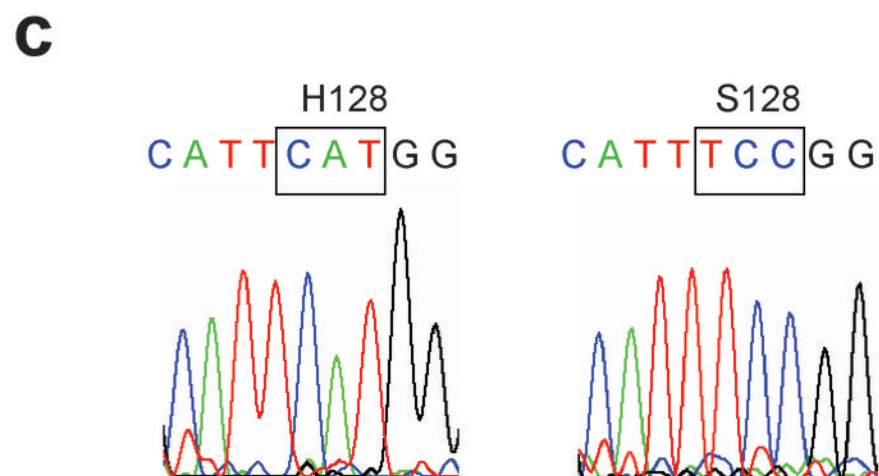
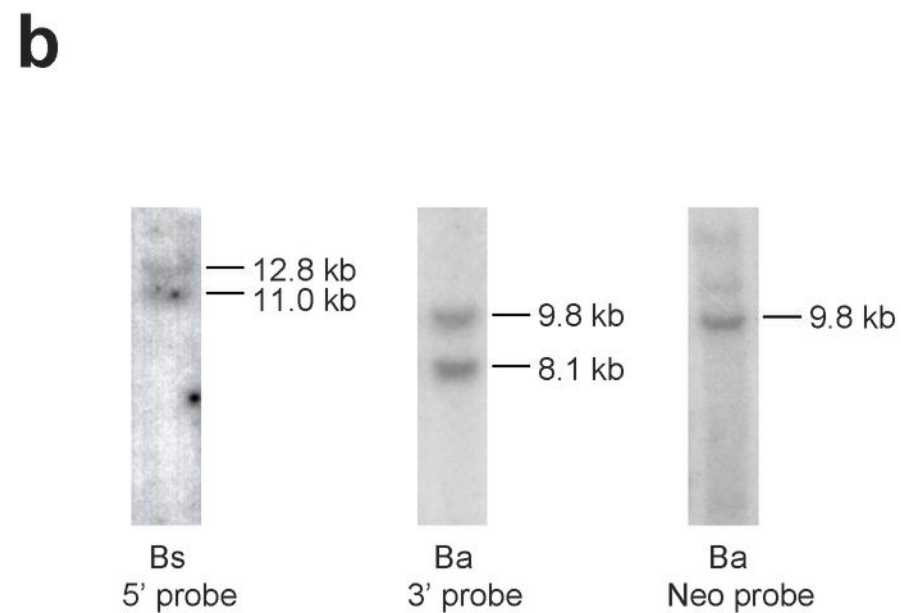
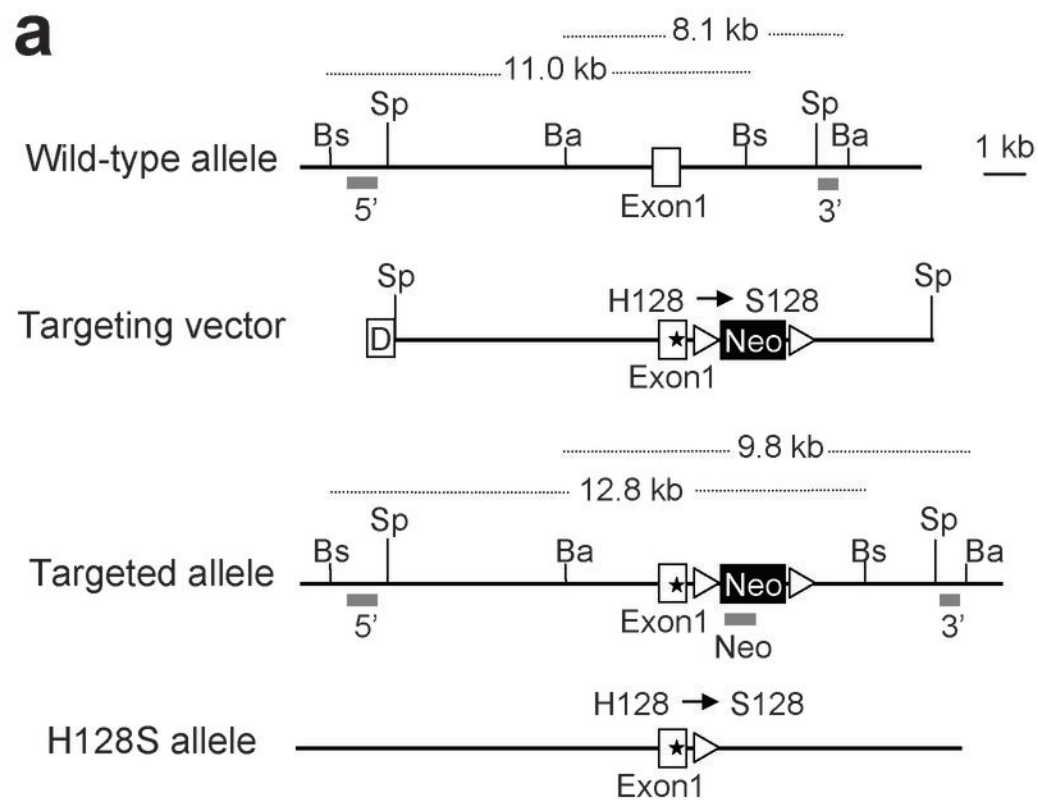
Statistical Analysis for behavioral measurements.

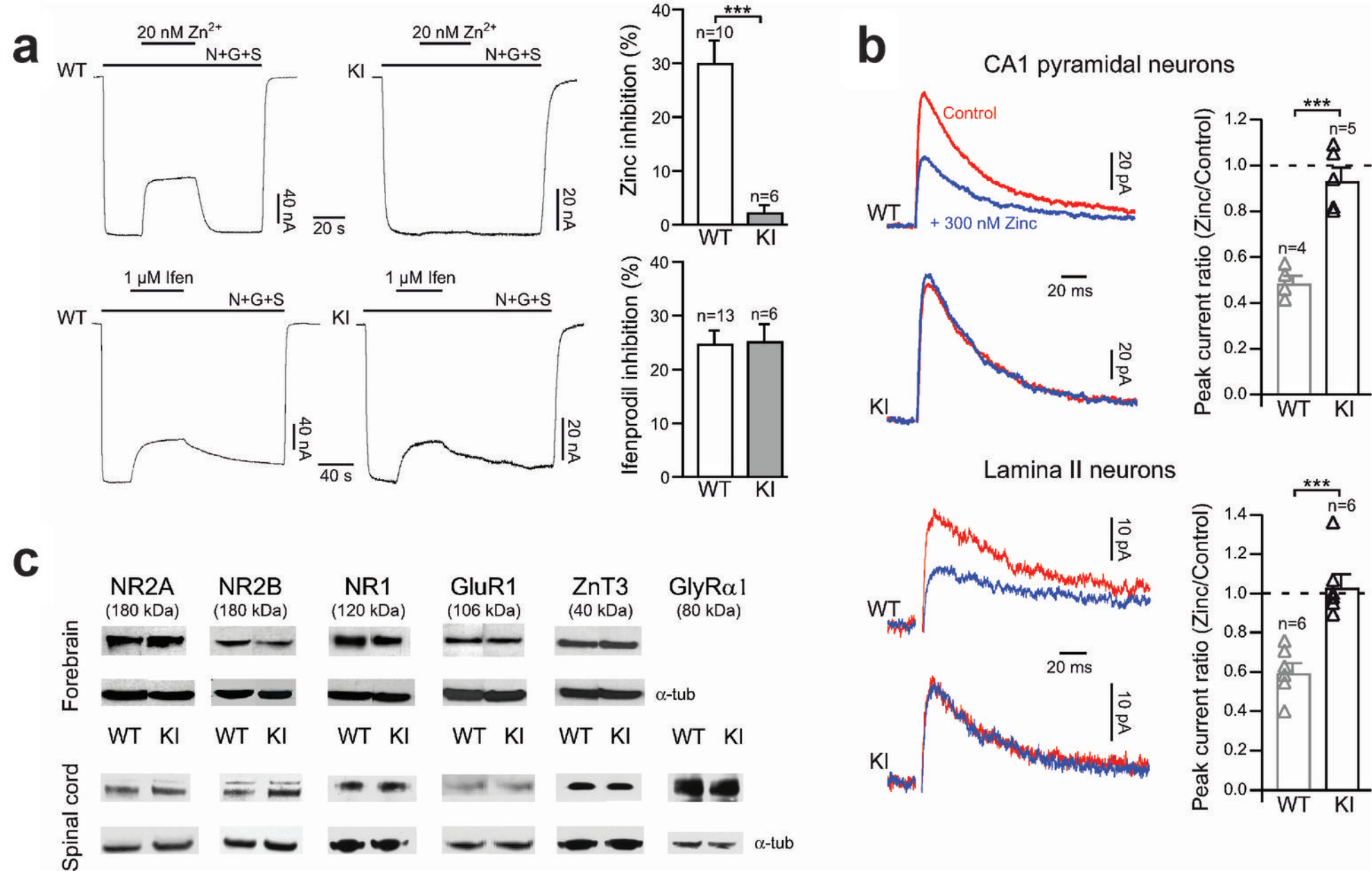
Neurological assessment. Data were analyzed by Student's *t*-test (except Rotarod and String tests) or non-parametric Mann-Whitney *U*-test.

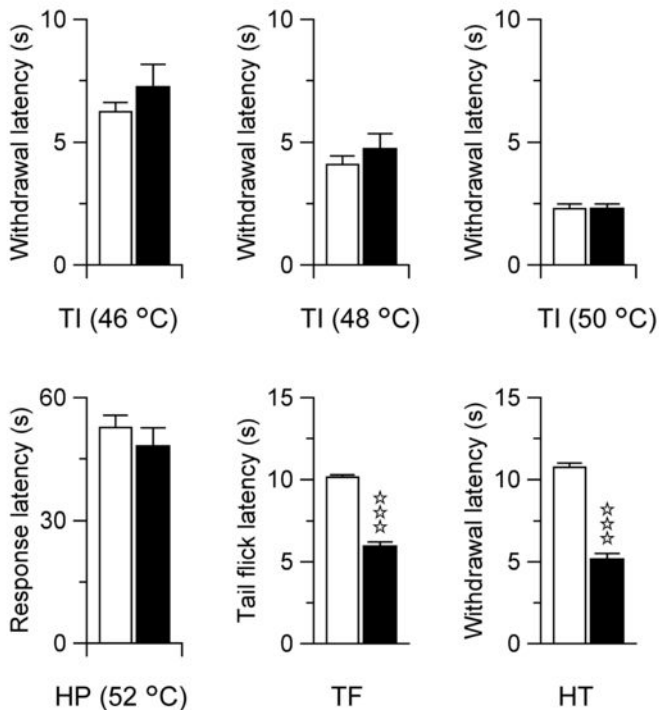
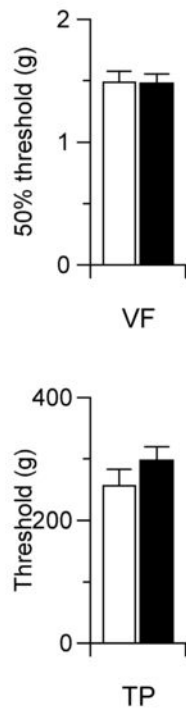
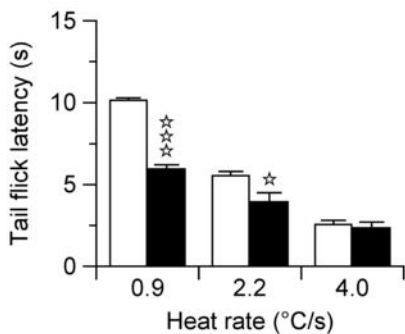
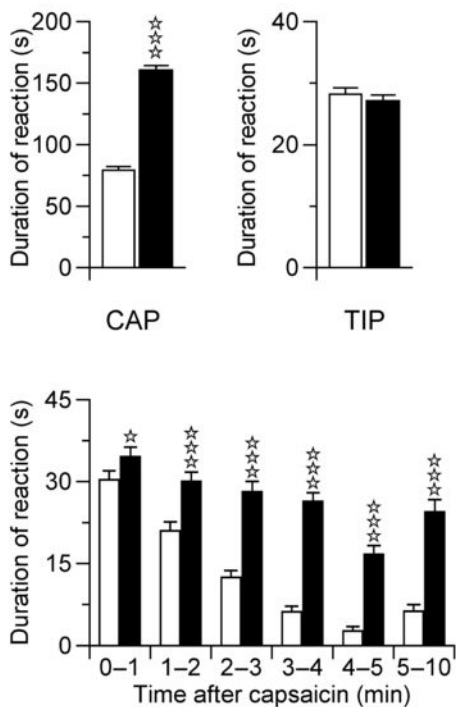
Locomotor habituation and circadian activity. Two-way ANOVA with genotype as the independent factor and time as the repeated measure was used. Student's *t*-test was used for individual group comparisons of total activity.

Pain. Comparison between genotypes for acute nociception, inflammatory and neuropathic pain was analyzed using repeated measures ANOVA followed by Student's *t*-test for individual time points when appropriate. The analysis of zinc pharmacology was performed using Two-way ANOVA for zinc effect and genotype followed by Bonferroni-dunn test.

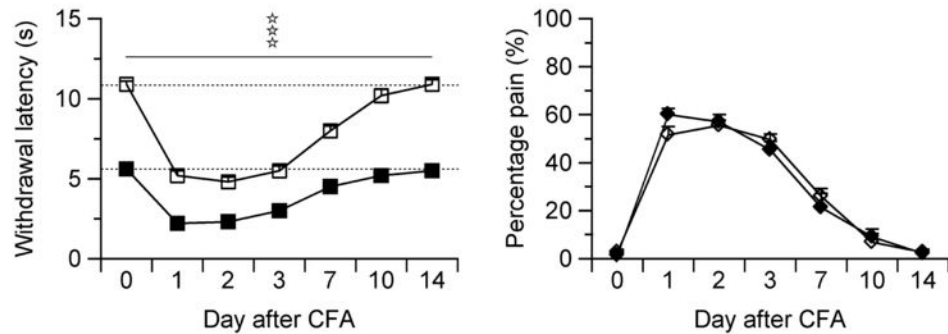
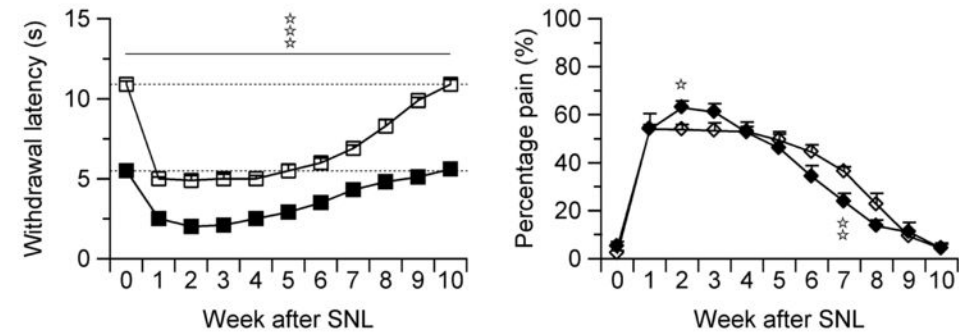
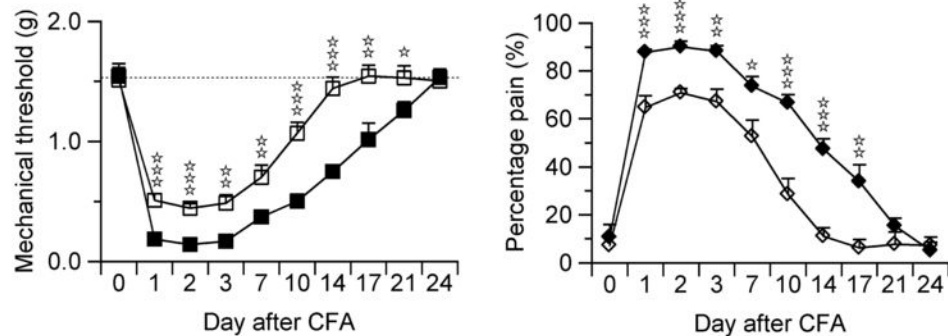
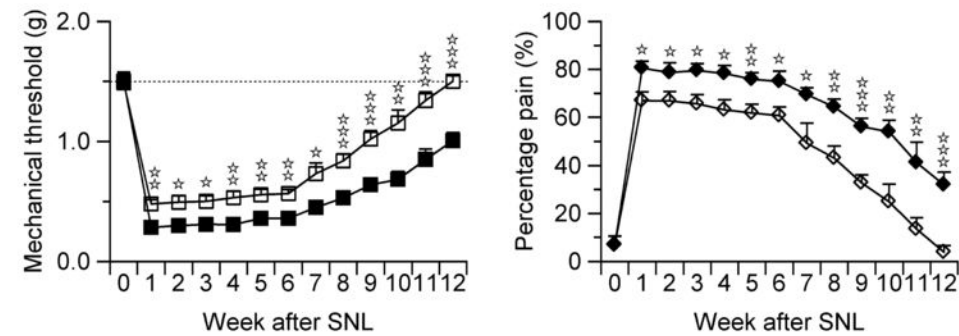
45. Miledi, R., Eusebi, F., Martinez-Torres, A., Palma, E. & Trettel, F. Expression of functional neurotransmitter receptors in *Xenopus* oocytes after injection of human brain membranes. *Proc Natl Acad Sci U S A* **99**, 13238-13242 (2002).
46. Boyce, S., *et al.* Selective NMDA NR2B antagonists induce antinociception without motor dysfunction: correlation with restricted localisation of NR2B subunit in dorsal horn. *Neuropharmacology* **38**, 611-623 (1999).
47. Ma, Q.P. & Hargreaves, R.J. Localization of N-methyl-D-aspartate NR2B subunits on primary sensory neurons that give rise to small-caliber sciatic nerve fibers in rats. *Neuroscience* **101**, 699-707 (2000).
48. Gaveriaux-Ruff, C., *et al.* Genetic ablation of delta opioid receptors in nociceptive sensory neurons increases chronic pain and abolishes opioid analgesia. *Pain* (2011).
49. Sakurada, T., Katsumata, K., Tan-No, K., Sakurada, S. & Kisara, K. The capsaicin test in mice for evaluating tachykinin antagonists in the spinal cord. *Neuropharmacology* **31**, 1279-1285 (1992).





a**b****c****d**

□ WT
 ■ KI

a Thermal pain**b** Thermal pain**c** Mechanical pain**d** Mechanical pain

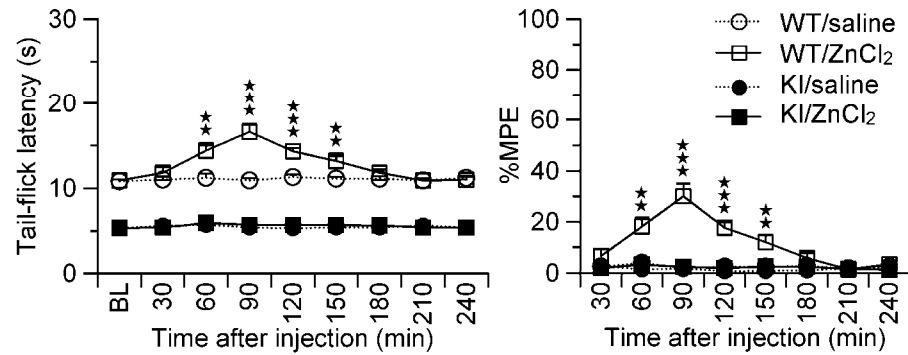
□ WT ■ KI

◇ WT ◆ KI

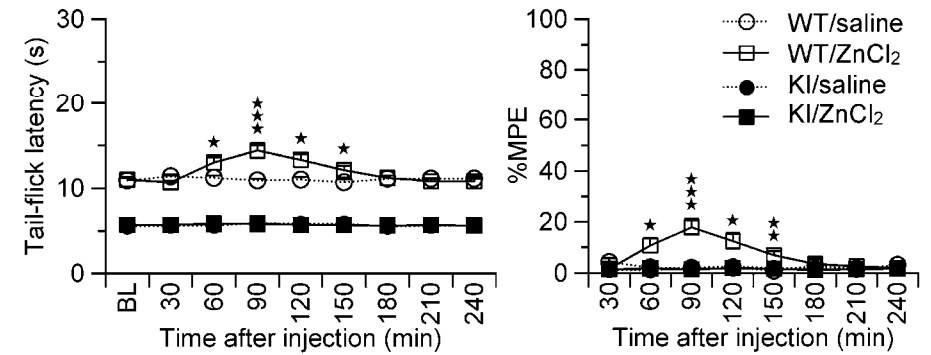
□ WT ■ KI

◇ WT ◆ KI

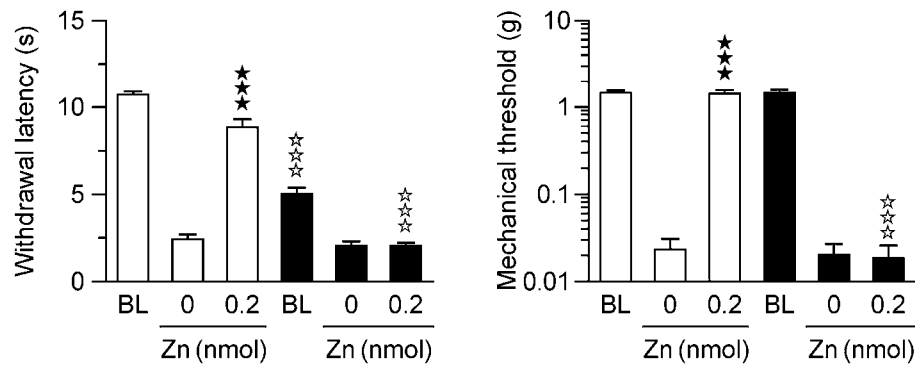
a Acute nociception - i.t. zinc



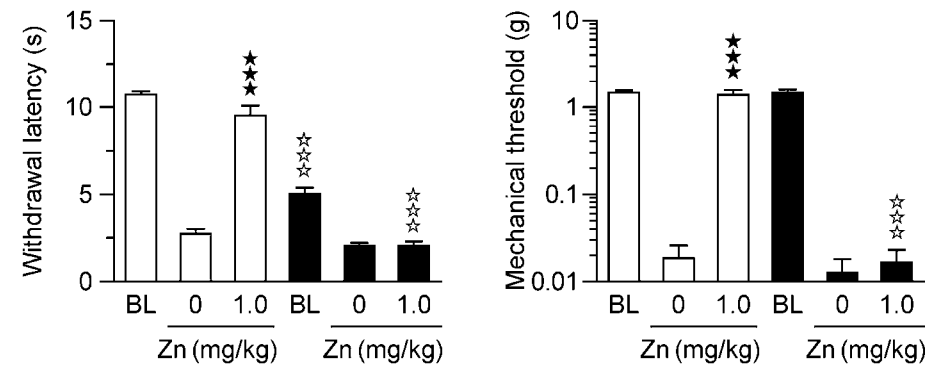
b Acute nociception - s.c. zinc



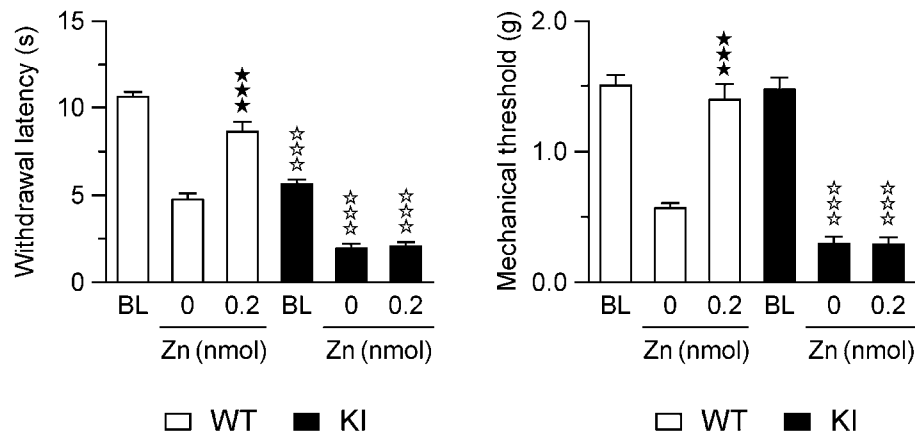
c CFA inflammatory pain - i.t. zinc



d CFA inflammatory pain - s.c. zinc



e SNL neuropathic pain - i.t. zinc



f SNL neuropathic pain - s.c. zinc

